

```
## Error in gzfile(file, "rb"): cannot open the connection
```

Is shrub expansion into grasslands pushed or pulled?

A spatial integral projection model for woody plant encroachment

Trevor Drees^{*a,b}, Brad M. Ochocki^b, Scott L. Collins^c, and Tom E.X. Miller^b

^aDepartment of Biology, Penn State University, State College, PA USA

^bProgram in Ecology and Evolutionary Biology, Department of BioSciences, Rice University, Houston, TX USA

^cDepartment of Biology, University of New Mexico, Albuquerque, NM USA

July 29, 2022

^{*}thd5066@psu.edu

Abstract

Encroachment¹ of shrubs into adjacent grasslands has become an increasingly reported phenomenon across the world, and such encroachment is either pulled forward by high population growth at the low-density encroachment front or pushed forward by higher-density areas behind the front. However, at sites such as Sevilleta National Wildlife Refuge in central New Mexico, little is known about whether encroachment is pushed or pulled, and the dynamics of encroachment are not well-understood. Here, long-term encroachment of creosotebush (*Larrea tridentata*), a native perennial shrub, stands in stark contrast with the stagnation in encroachment observed in recent decades. In order to better understand creosotebush encroachment at this site, we quantify it using a spatially structured population model where a wave of individuals travels at a speed governed by both dispersal and density-dependence. Results indicate that population growth rates generally increase with decreasing density, suggesting that encroachment is pulled by individuals at the low-density wave front, and the spatial population model predicts an encroachment rate of less than 2 cm per year. While the predicted rate of encroachment is consistent with observations over recent decades, it does not explain long-term creosotebush encroachment at the study site, suggesting that this process may occur in pulses when recruitment, seedling survival, or dispersal significantly exceed typical rates. Overall, our work demonstrates that individuals at low densities are likely the biggest contributors to creosotebush encroachment at this site, and that this encroachment is likely a process that occurs in large but infrequent bursts rather than at a steady pace.

¹*I am not editing the abstract for now.*

23

Keywords

24 density-dependence, ecotones, woody encroachment, shrubs, integral projection model,
25 grassland

Introduction

The recent and ongoing encroachment of shrubs and other woody plants into adjacent grasslands has caused significant vegetation changes across arid and semi-arid landscapes worldwide (Cabral et al., 2003; Gibbens et al., 2005; Goslee et al., 2003; Parizek et al., 2002; Roques et al., 2001; Trollope et al., 1989; Van Auken, 2009, 2000). The process of encroachment generally involves increases in the number or density of woody plants in both time and space (Van Auken, 2000), which can drive shifts in plant community structure and alter ecosystem processes (Knapp et al., 2008; Ravi et al., 2009; Schlesinger and Pilmanis, 1998; Schlesinger et al., 1990). Other effects of encroachment include changes in ecosystem services (Kelleway et al., 2017; Reed et al., 2015), declines in biodiversity (Brandt et al., 2013; Ratajczak et al., 2012; Sirami and Monadjem, 2012), and economic losses in areas where the proliferation of shrubs adversely affects grazing land and pastoral production (Mugasi et al., 2000; Oba et al., 2000).

Woody plant encroachment can be studied through the lens of spatial population biology as a wave of individuals that may expand across space and over time (Kot et al., 1996; Neubert and Caswell, 2000; Pan and Lin, 2012; Wang et al., 2002). Theory predicts that the speed of wave expansion depends on two processes: local demography and dispersal of propagules. First, local demographic processes include recruitment, survival, growth, and reproduction, which collectively determine the rate at which newly colonized locations increase in density and produce new propagules. Second, colonization events are driven by the spatial dispersal of propagules, which is commonly summarized as a probability distribution of dispersal distance, or “dispersal kernel”. The speed at which expansion waves move is highly dependent upon the shape of the dispersal kernel, especially long-distance dispersal events in the tail of the distribution (Skarpaas

50 and Shea, 2007). Both demography and dispersal may depend on plant size, since larger
51 plants often have improved demographic performance and release seeds from greater
52 heights, leading to longer dispersal distances (Nathan et al., 2011). Accounting for popu-
53 lation structure, including size structure, may therefore be important for understanding
54 and predicting wave expansion dynamics (Neubert and Caswell, 2000).

55 Theory predicts that the nature of conspecific density dependence is another critical
56 feature of expansion dynamics but this is rarely studied in the context of woody plant
57 encroachment. Expansion waves typically correspond to gradients of conspecific density
58 – high in the back and low at the front – and demographic rates may be sensitive to den-
59 sity due to intraspecific interactions like competition or facilitation. If the demographic
60 effects of density are strictly negative due to competitive effects that increase with den-
61 sity then demographic performance is maximized as density goes to zero, at the leading
62 edge of the wave. Under these conditions, the wave is “pulled” forward by individuals
63 at the low-density vanguard (Kot et al., 1996), and targeting these individuals and lo-
64 cations would be the most effective way to slow down or prevent encroachment (cite?).
65 However, woody encroachment systems often involve positive feedbacks whereby shrub
66 establishment modifies the environment in ways that facilitate further shrub recruit-
67 ment. For example, woody plants can modify their micro-climates in ways that elevate
68 nighttime minimum temperatures, promoting conspecific recruitment and survival for
69 freeze-sensitive species (D’Odorico et al., 2010; Huang et al., 2020). Positive density de-
70 pendence (or Allee effects) causes demographic rates to be maximized at higher densities
71 behind the leading edge, which “push” the expansion forward, leading to qualitatively
72 different expansion dynamics (Keitt et al., 2001; Kot et al., 1996; Lewis and Kareiva, 1993;
73 Sullivan et al., 2017; Taylor and Hastings, 2005; Veit and Lewis, 1996). Pushed expan-
74 sion waves generally have different shapes (steeper density gradients) and slower speeds

75 than pulled waves (Gandhi et al., 2016), and may require different strategies for manag-
76 ing or decelerating expansion (check Taylor and Hastings ref). The potential for positive
77 feedbacks is well documented in woody encroachment systems but it remains unclear
78 whether and how strongly these feedbacks decelerate shrub expansion and influence
79 strategies for management of woody encroachment.

80 In this study, we linked woody plant encroachment to ecological theory for inva-
81 sion waves, with the goals of understanding how seed dispersal and density-dependent
82 demography drive encroachment, and determining whether the encroachment wave is
83 pushed or pulled. Throughout the aridlands of the southwestern United States, shrub
84 encroachment into grasslands is well documented (D’Odorico et al., 2012) but little is
85 known about the dispersal and demographic processes that govern it. Our work fo-
86 cused on encroachment of creosotebush (*Larrea tridentata*) in the northern Chihuahuan
87 Desert. Expansion of this species into grasslands over the past 150 years has been well
88 documented, leading to decreased cover of *Bouteloua eriopoda*, the dominant foundation
89 species of Chihuahuan desert grassland (Buffington and Herbel, 1965; Gardner, 1951;
90 Gibbens et al., 2005). As in many woody encroachment systems, creosotebush expansion
91 generates ecotones marking a transition from dense shrubland to open grassland, with a
92 transition zone in between where shrubs can often be found interspersed among grasses
93 (Fig. 1).

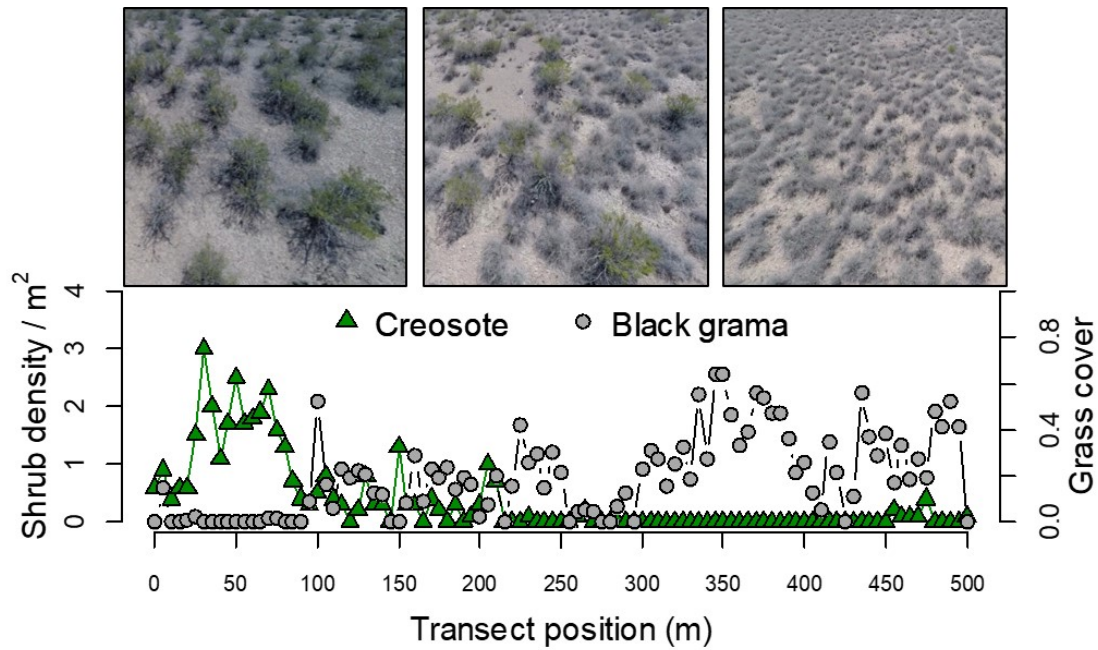


Figure 1: Example of an ecotone transect at Sevilleta LTER, spanning gradients of creosotebush and black grama grass. Photo credits: TEX Miller

Historically, creosotebush encroachment into grasslands is believed to have been driven by a combination of factors including overgrazing, drought, variability in rainfall, and suppression of fire regimes Moreno-de las Heras et al. (2016). These shrubs are also thought to further facilitate their own encroachment through positive feedbacks (D'Odorico et al., 2012; Grover and Musick, 1990) by modifying their environment in ways that favor continued growth and recruitment, including changes to the local microclimate (D'Odorico et al., 2010) and rates of soil erosion (Turnbull et al., 2010). Such positive feedback also involve suppression of herbaceous competitors, reducing competition as well as the amount of flammable biomass used to fuel the fires that keep creosotebush growth in check (Van Auken, 2000). We hypothesized that, given potential for positive

104 feedback mechanisms, the rarity of conspecifics at the low-density encroachment front
105 may depress demographic performance and generate pushed-wave dynamics.

106 We used a combination of observational and experimental data from shrub ecotones
107 in central New Mexico to parameterize a spatial integral projection model (SIPM) that
108 predicts that speed of encroachment (m/yr) resulting from lower-level demographic and
109 dispersal processes. Our data came from demographic surveys and experimental trans-
110 plants along replicate ecotone transects spanning a gradient of shrub density, and seed
111 drop experiments to estimate the properties of the dispersal kernel. We focused on wind
112 dispersal of seeds, since little is known about the natural history of dispersal in this sys-
113 tem and the seeds lack rewards to attract animal dispersers. We also used re-surveys
114 of permanent transects as an independent measure of encroachment that provided a
115 benchmark against which to evaluate model predictions. The SIPM accounts for size-
116 structured demography of creosotebush, allows us to test whether shrub expansion is
117 pulled by the low-density front or pushed from the high-density core, and identifies the
118 local (demographic) and spatial (seed dispersal) life cycle transitions that most strongly
119 contribute to expansion speed². We address the following specific questions:

- 120 1. What is the nature of conspecific density dependence in demographic vital rates
121 along shrub encroachment ecotones? Is encroachment pulled by the individuals at
122 the front or pushed by individuals behind it?
- 123 2. What is the seed dispersal kernel for this species and how does this vary with
124 maternal plant size?
- 125 3. What is the predicted rate of expansion from the SIPM and which lower-level pro-
126 cesses most strongly affect the expansion speed?

²*we will need to stay consistent with the language of encroachment/expansion/invasion. For now I am switching a lot.*

127 4. How does the observed rate of encroachment in the recent past compare to model
128 predictions?

129 **Materials and methods**

130 *Study species*

131 Creosotebush *Larrea tridentata* is a perennial, drought-resistant shrub that is native to
132 the arid and semiarid regions of the southwestern United States and northern Mexico.
133 High-density areas of creosotebush consist largely of barren soil between plants due to
134 the “islands of fertility” these shrubs create around themselves (Reynolds et al., 1999;
135 Schlesinger et al., 1996), though lower-density areas will often contain grasses in the
136 inter-shrub spaces (Fig. 1). In our northern Chihuahuan desert study region creosote-
137 bush reproduces sexually, with numerous small yellow flowers giving rise to highly
138 pubescent spherical fruits several millimetres in diameter; these fruits consist of five
139 carpels, each of which contains a single seed. Seeds are dispersed from the parent plant
140 by gravity and wind, with the possibility for seeds to subsequently be transported by
141 animals or water (Maddox and Carlquist, 1985). In other regions, this species also repro-
142 duces asexually and can give rise to long-lived clonal stands (Vasek, 1980), but this does
143 not occur in our study region. The foliage is dark green, resinous, and unpalatable to
144 most grazing and browsing animals (Mabry et al., 1978).

145 *Study site*

146 We conducted our work at the Sevilleta National Wildlife Refuge (SNWR), a Long-Term
147 Ecological Research (SEV-LTER) site in central New Mexico. The refuge exists at the in-
148 tersection of several eco-regions, including the northern Chihuahuan Desert, Great Plains

149 grassland, and steppes of the Colorado Plateau. Annual precipitation is approximately
150 250 mm, with the majority falling during the summer monsoon season from June to
151 September. The recruitment events that facilitate creosotebush expansion are thought
152 to be highly episodic (Peters and Yao, 2012), and this may be linked to fluctuations in
153 monsoon precipitation (Bowers et al., 2004; Boyd and Brum, 1983). Monsoon precipitation
154 during the study years (2013-2017) was [summarise climate data].

155 *Demographic data*

156 *Ecotone transects*

157 We collected demographic data during early June of every year from 2013-2017. This
158 work was conducted at **four sites in the eastern part of SNWR**³ (one site was initiated
159 in 2013 and the other three in 2014), with three transects at each site. All transects were
160 situated along a shrubland-grassland ecotone so that a full range of shrub densities was
161 captured: each transect spanned core shrub areas, grassland with no or few shrubs,
162 and the transition between them. Lengths of these transects varied from 200 to 600 m,
163 determined by the strength of vegetation transition since “steep” transitions required
164 less length to capture the full range of shrub density.

165 We quantified shrub density in 5-meter “windows” along each transect, including all
166 shrubs within one meter of the transect on either side (shrubs that partially overlapped
167 with the census area were included). Densities were quantified once for each transect
168 (in 2013 or 2014) and were assumed to remain constant for the duration of the study, a
169 reasonable assumption for a species with very low recruitment and very high survival
170 of established plants. Given the population’s size structure, we weighted the density of
171 each window by the sizes of the plants, which we quantified as volume (cm³). Volume

³would a map be helpful?

172 was calculated as that of an elliptic cone: $V_i = \frac{\pi h}{3} \frac{lw}{4}$ where l , w , and h are the max-
173 imum length, maximum width, and height, respectively. Maximum length and width
174 were measured so that they were always perpendicular to each other, and height was
175 measured from the base of the woody stem at the soil surface to the tallest part of the
176 shrub. The weighted density for a window was then expressed as $\log(\text{volume})$ summed
177 over all plants in the window.

178 *Observational census*

179 At approximately 50-m intervals along each transect we tagged up to 10 plants for annual
180 demographic census and recorded their local (5-m resolution) window so that we could
181 connect individual demographic performance to local density. These tagged shrubs were
182 revisited every June and censused for survival (alive/dead), size (width, length, and
183 height, as above), flowering status, and fertility of flowering plants (numbers of flower-
184 buds, flowers, and fruits). In instances where shrubs had large numbers of reproductive
185 structures that would be difficult to reliably count (a large shrub may have thousands of
186 flowers or fruits), we made counts on a fraction of the shrub and extrapolated to esti-
187 mate whole-plant reproduction. Creosotebush does not have one discrete reproductive
188 event per year; instead, flowering may occur throughout much of the warm season. By
189 combining counts of buds, flowers, and fruits we intended to capture a majority of the
190 season's reproductive output, assuming that all buds and flowers will eventually become
191 fruits. Our measurements of reproductive output are therefore conservative and may un-
192 derestimate total seed production for an entire transition year. Each year, we searched
193 for new recruits within one m on either side of the transect. New recruits were tagged
194 and added to the demographic census. The observational census included a total of 522
195 unique individuals.

196 *Transplant experiment*

197 We conducted a transplant experiment in 2015 to test how shrub density affects seedling
198 survival. This approach complemented observational estimates of density dependence
199 and filled in gaps for a part of the shrub life cycle that was rarely observed due to low
200 recruitment. Seeds for the experiment were collected from plants in our study popu-
201 lation in 2014. Seeds were germinated on Pro-Mix potting soil (Quakertown, PA) in
202 Fall 2014 and seedlings were transferred to 3.8 cm-by-12.7 cm cylindrical containers and
203 maintained in a greenhouse at Rice University. Seedlings were transported to SNWR
204 and transplanted into the experiment during July 27-31, 2015. Transplant timing was
205 intended to coincide with the monsoon season, when most natural recruitment occurs.

206 The transplant experiment was conducted at the same four sites and three transects
207 per site as the observational demographic census, where we knew weight shrub densities
208 at 5-m window resolution. We established 12 1-m by 1-m plots along each transect. Plots
209 were intentionally placed to capture density variation: four plots were in windows with
210 zero shrubs, four plots were placed in the top four highest-density windows on the
211 transect, and the remaining four plots were randomly distributed among the remaining
212 windows with weighted density greater than zero. Plots were placed in the middle of
213 each 5-m window (at meter 2.5) and were divided into four 0.5-m by 0.5-m subplots.
214 We divided each subplot into nine squares (0.125-m by 0.125-m) and recorded ground
215 cover of each square as one of the following categories: bare ground, creosotebush,
216 black grama (*B. eriopoda*), blue grama (*B. gracilis*), other grass, or “other”. Each subplot
217 received one transplanted shrub seedling, for a total of 48 transplants per transect, 144
218 transplants per site, and 576 transplants in the entire experiment. Each site was set
219 up on a different day and there was a significant monsoon event after the third and
220 before the fourth site. This resulted in differential mortality that appears to be related

221 to site (captured as a statistical random effect) but more likely reflects the timing of the
222 monsoon event relative to planting (moist soil likely promoted transplant survival). We
223 revisited the transplant experiment on October 24, 2015 to survey mortality. After that
224 first visit, transplants were censused along with the naturally occurring plants each June,
225 following the methods described above.

226 *Demographic analysis*

227 We fit statistical models to the demographic data and used AIC-based model selection to
228 evaluate empirical support for alternative candidate models. The top statistical models
229 were then used as the vital rate sub-models of the SIPM, so there is a strong connection
230 between the statistical and population modeling, as is typical of integral projection mod-
231 eling. Our analyses focused on the following demographic vital rates: survival, growth,
232 probability of flowering, fertility (flower and fruit production), seedling recruitment, and
233 seedling size. Most of these vital rates were modeled as a function of plant size, and all
234 of them included the possibility of density dependence.

235 The alternative hypotheses of pushed versus pulled wave expansion rest on how the
236 rate of population increase (λ), derived from the combination of all vital rates, respond
237 to density. We were particularly interested in whether demographic performance was
238 maximized as local density goes to zero (pulled) or at non-zero densities behind the
239 wave front (pushed). To flexibly model density dependence and detect non-monotonic
240 responses, we used generalized additive models in the R package ‘mgcv’ (Wood, 2017).
241 For each vital rate, we fit candidate models with or without a smooth term for local
242 weighted density (among other possible covariates). To avoid over-fitting, we set the
243 ‘gamma’ argument of gam() to 1.8, which increases the complexity penalty, results in
244 smoother fits (Wood, 2017), and makes our approach more conservative (other gamma

values yielded qualitatively similar results). We pooled data across transition years for analysis. All models included the random effect of transect (12 transects across 4 sites); we did not attempt to model both site and transect-within-site random effects due to the low numbers of each. All vital rate functions used the natural logarithm of volume (cm^3) as the size variable and the sum of $\log(\text{volume})$ as the weighted density of a transect window.

Survival. We modeled survival or mortality in year $t + 1$ as a Bernoulli random variable with three candidate models for survival probability. These included smooth terms for initial size in year t only (1), initial size and weighted density (2), and both smooth terms plus an interaction between initial size and weighted density (3). We analyzed survival of experimental transplants and observational census plants together in the same analyses, with a fixed effect of transplant status (yes/no) included in all candidate models. Since recruits and thus mortality events were both very rare in the observational survey, this approach allowed us to “borrow strength” over both data sets to generate a predictive function for size- and possibly density-dependent survival while statistically accounting for differences between experimental and naturally occurring plants. Because we had additional, finer-grained cover data for the transplant experiment that we did not have for the observational census, we conducted an additional stand-alone analysis of transplant survival that explored the influence of shrub and grass density at multiple spatial scales (Appendix).

Growth. We modeled size in year $t + 1$ as a Gaussian random variable. There were nine candidate models for growth. The simplest model (1) defined the mean of size in year $t + 1$ as a smooth function of size in year t and constant variance. Models (2) and (3) had constant variance but the mean included smooth terms for initial size and weighted

269 density (2) or both smooth terms plus an interaction between initial size and weighted
270 density (3). Models 4-6 had the same mean structure as 1-3 but defined the standard
271 deviation of size in year $t + 1$ as a smooth function of initial size. Models 7-9 mirrored 4-6
272 and additionally included a smooth term for weighted density in the standard deviation.
273 Modeling growth correctly is important because it defines the probability of any future
274 size conditional on current size, a critical element of the IPM transition kernel. We
275 verified that the AIC-selected model described the data well by simulating data from it
276 and comparing the moments (mean, variance, skewness, and kurtosis) of simulated and
277 real data.

278 *Flowering and fruit production.* We modeled shrub reproductive status (vegetative or
279 flowering) in year t as a Bernoulli random variable with three candidate models for
280 flowering probability. These included smooth terms for current size (in year t) only (1),
281 size and weighted density (3), and both smooth terms plus an interaction between size
282 and weighted density. We modeled the reproductive output of flowering plants (the sum
283 of flowerbuds, open flowers, and fruits) in year t as a negative binomial random variable.
284 There were three candidate models for mean reproductive output that corresponded to
285 the same three candidates for flowering probability.

286 *Recruitment and recruit size.* We modeled seedling recruitment in each transect window
287 as a binomial random variable given the number of total seeds produced in that window
288 in the preceding year. There were two candidate models, with and without an influence
289 of weighted density on the per-seed recruitment probability. To estimate window-level
290 seed production, we used the best-fit models for flowering and fruit production and
291 applied this to all plants in each window that we observed in our initial density surveys.
292 We assume that recruits come from the previous year's seeds and not from a long-lived

293 soil seed bank.

294 We modeled recruit size as a Gaussian-distributed random variable and fit four can-
295 didate models including an influence of weighted density on mean, variance, both, and
296 neither.

297 *Density-dependent IPM*

298 The size- and density-dependent statistical models comprised the sub-models of a den-
299 sity dependent Integral Projection Model (IPM) that we used to evaluate how the shrub
300 population growth rate responded to con-specific density; we present this non-spatial
301 model before layering on the spatial dynamics generated by seed dispersal. A basic
302 density-independent IPM predicts the number of individuals of size x' at time $t + 1$
303 ($n(x', t + 1)$) based on a demographic projection kernel (K_{dem}) that gives the rates of tran-
304 sition from sizes x to x' from times t to $t + 1$ and is integrated over the size distribution
305 from the minimum (L) to maximum (U) sizes. In a density-dependent IPM, components
306 of the projection kernel may respond to population abundance and structure:

$$307 \quad n(x', t + 1) = \int_L^U K_{dem}(x', x, \tilde{n}(t)) n(x, t) dx \quad (1)$$

308 Here, $\tilde{n}(t)$ is some function of population structure $n(x, t)$ such as the total density of
309 conspecifics ($\tilde{n}(t) = \int n(x, t) dx$) or, as in our case, total density weighted by size ($\tilde{n}(t) =$
310 $\int x n(x, t) dx$). For simplicity, in the analyses that follow we do not model density as
311 a dynamic state variable; instead, we treat density as a static covariate ($\tilde{n}(t) = \tilde{n}$) and
312 evaluate the IPM at a range of density values. As in our statistical modeling, the size
313 variable of the IPM (x, x') was $\log(\text{cm}^3)$.

314 For our model, the size- and density-dependent demographic transitions captured by
315 the projection kernel include growth or shrinkage (g) from size x to x' conditioned on

survival (s) at size x (combined growth-survival function $G(x', x, \tilde{n}) = g(x', x, \tilde{n})s(x, \tilde{n})$),
 and the production of new size- x' individuals from size- x parents ($Q(x', x, \tilde{n})$). Repro-
 duction reflects the probability of flowering at size x (p), the number of seeds produced
 by flowering plants (d), the per-seed probability of recruitment (r), and the size distribu-
 tion of recruits (c). Collectively, the rate at which x -sized individuals produce x' -sized
 individuals at density \tilde{n} is given by the combined reproduction-recruitment function
 $Q(x', x, \tilde{n}) = p(x, \tilde{n})d(x, \tilde{n})r(\tilde{n})c(x', \tilde{n})$. Thus, we can express the projection kernel as:

$$K_{dem}(x', x, \tilde{n}) = G(x', x, \tilde{n}) + Q(x', x, \tilde{n}) \quad (2)$$

For analysis, we evaluated the IPM kernel over a range of local densities from the mini-
 mum to the maximum of weighted density values from the 5-meter windows ($0 \leq \tilde{n} \leq$
 \tilde{n}_{max}). At each density level, we discretized the IPM kernel into a 200×200 approxim-
 ating matrix and calculated the asymptotic growth rate $\lambda(\tilde{n})$ as its leading eigenvalue. We
 extended the lower (L) and upper (U) integration limits to avoid unintentional “eviction”
 using the floor-and-ceiling method (Williams et al., 2012).

We sought to characterize the shape of density dependence: whether fitness declined
 monotonically or not with increasing density. We quantified uncertainty in the density-
 dependent growth rate $\lambda(\tilde{n})$ by bootstrapping our data. For each bootstrap, we ran-
 domly sampled 75% of our demographic data, re-ran the statistical modeling and model
 selection, and used the top vital rate models to generate $\lambda(\tilde{n})$ for that data subset. We
 repeated this procedure for 500 bootstrap replicates.

Dispersal modelling

WALD dispersal model. Dispersal kernels were calculated using the WALD, or Wald analytical long-distance dispersal, model that uses a mechanistic approach to predict dispersal patterns of plant propagules by wind. The WALD model, which is based in fluid dynamics, can serve as a good approximation of empirically-determined dispersal kernels (Katul et al., 2005; Skarpaas and Shea, 2007) and may be used when direct observations of dispersal are not available. Under the assumptions that wind turbulence is low, wind flow is vertically homogenous, and terminal velocity is achieved immediately upon seed release, the WALD model simplifies a Lagrangian stochastic model to create a dispersal kernel that estimates the likelihood a propagule will travel a given distance (Katul et al., 2005). Our dispersal kernel takes the form of the inverse Gaussian distribution

$$p(r) = \left(\frac{\lambda'}{2\pi r^3} \right)^{\frac{1}{2}} \exp \left[-\frac{\lambda'(r - \mu')^2}{2\mu'^2 r} \right] \quad (3)$$

that is a slight adaptation⁴ from equation 5b in Katul et al. (2005), using r to denote dispersal distance. Here, λ' is the location parameter and μ' is the scale parameter, which depend on environmental and plant-specific properties of the study system. (We use λ' for consistency with notation in related papers, but λ' the dispersal location parameter should not be confused with λ the geometric growth rate.) The location and scale parameters are defined as $\lambda' = (H/\sigma)^2$ and $\mu' = HU/F$; these are functions of the height H of seed release, wind speed U at seed release height, seed terminal velocity F , and the turbulent flow parameter σ that depends on both wind speed and local vegetation roughness. We parameterized the WALD dispersal kernel using windspeed data from the SEV-LTER weather station nearest our study site (Moore and Hall, 2022) and seed

⁴unclear what this refers to

terminal velocity data from laboratory-based seed-drop experiments (Appendix A). We integrated the dispersal kernel over observed variation in wind speeds, seed terminal velocity, and release height within the height of a shrub. Therefore the dispersal kernel for a shrub of height U was given by:

$$K_{disp} = \iiint p(F)p(U)p(z)p(r) dF dU dz \quad (4)$$

and $p(F)$ and $p(U)$ are the PDFs of the terminal velocity F and wind speed U , respectively, and $p(z)$ is the uniform distribution from the minimum seed release height ($0.15m$, the height at which grass cover interferes with wind dispersal) to H . Methods for our seed data collection and technical details of dispersal kernel modeling are provided in Appendix A.

Spatial integral projection model

We used a spatial integral projection model to piece together seed dispersal and density-dependent demography, and generate predictions for the rate of shrub expansion that results from this combination of local and spatial processes. The spatially explicit model builds upon the non-spatial model (Eq. 1) and adds a spatial variable (z, z') such that demographic transitions occur across both time and space according to a combined demography-dispersal kernel \tilde{K} :

$$n(x', z', t + 1) = \int_{-\infty}^{+\infty} \int_L^U \tilde{K}(x', x, z', z, \tilde{n}(z, t)) n(x, z, t) dx dz \quad (5)$$

Here, $\tilde{K}(x', x, z', z, \tilde{n}(z, t))$ describes the transition from size x and location z to size x' and location z' given density $\tilde{n}(z, t)$ at starting location z . As before, \tilde{n} is a function of population structure – in our model, weighted local density – but here integrated

over an explicit competitive “neighborhood”: $\tilde{n}(z, t) = \int_{z-h}^{z+h} \int_L^U x n(x, z, t) dx dz$ where h represents neighborhood size in the units of z . The demography-dispersal kernel \tilde{K} is given by the sum of two parts, one that describes reproduction coupled with dispersal of propagules, and another that describes growth and survival of non-dispersing individuals:

$$\tilde{K}(x', x, z', z, \tilde{n}(z, t)) = K_{disp}(z' - z)Q(x', x, \tilde{n}) + \delta(z' - z)G(x', x, \tilde{n}) \quad (6)$$

Here, regeneration function Q and growth-survival function G correspond to Eq. 2, dispersal kernel K_{disp} corresponds to Eq. , and the Dirac delta function is a probability distribution with all mass at zero, which prevents movement. Following standard assumptions for integro-difference equations, we assume that space is one-dimensional and homogeneous, such that demographic transitions do not depend on location (or, more precisely, that they depend on location only through spatial variation in density) and the probability of dispersing from location z to z' depends only on the absolute distance between them.

Under many conditions, models of this form generate traveling waves, and we are particularly interested in the velocity (m/yr) of this wave. Methods to estimate this velocity depend strongly on how demography responds to density. If fitness is maximized at some density $\tilde{n} > 0$ then the wave is pushed and wave velocity can only be estimated through numerical simulation. However, if fitness is maximized at $\tilde{n} = 0$ then the wave is pulled and an upper bound on its asymptotic velocity can be calculated analytically, following Neubert and Caswell (2000) and Jongejans et al. (2011), as

$$c^* = \min_{s>0} \left[\frac{1}{s} \ln(\rho_s) \right] \quad (7)$$

401 where s is a wave shape parameter and ρ_s is the dominant eigenvalue of the kernel
 402 $H_s(x', x)$. Corresponding to Eq. 6 and assuming $\tilde{n} = 0$, H_s is composed of

$$403 \quad H_s(x', x) = M(s, x)Q(x', x) + G(x', x) \quad (8)$$

404 where $M(s, x)$ is the moment-generating function (MGF) for the dispersal kernel as-
 405 sociated with size x . This formulation of the model assumes that the dispersal kernel
 406 depends only on maternal size x and not offspring size x' . To estimate $M(s, x)$ we sim-
 407 ulated $N = 10000$ dispersal events (r) for each size x and marginalized these over one
 408 spatial dimension as in Lewis et al. (2006). We then evaluated the empirical MGF for
 409 each size x : $M(s) = \frac{1}{N} \sum_{i=1}^N e^{sr}$.

410 We used numerical sensitivity analysis to compare the contributions of demography
 411 and dispersal processes to the speed of expansion. We perturbed each vital rate function
 412 by an arbitrary value, recalculated wavespeed, and quantified sensitivity as the change
 413 in wavespeed divided by the perturbation. Analytical sensitivity analysis is also possible
 414 (Ellner et al., 2016) but these sensitivities reflect infinitesimally small perturbations. We
 415 were particularly interested in the effects of large perturbations, especially large changes
 416 in seedling recruitment, which is subject to pulse events.

417 Estimates of wavespeed and its sensitivity to demography and dispersal processes
 418 were bootstrapped for a total of 1000 replicates. Each bootstrap replicate recreated size-
 419 and density-dependent demographic models using 50% resampling on the original de-
 420 mographic data, and recreated dispersal kernels also using 50% resampling on the wind
 421 speeds and seed terminal velocities. Model selection for demographic vital rates was re-
 422 run for each bootstrap replicate. The empirical MGF relied on numerical sampling and
 423 was therefore sensitive to extreme long-distance events that differed across bootstrap
 424 realizations. Therefore, bootstrapped distributions reflect the combination of model un-

425 certainty, parameter uncertainty, and stochasticity inherent to empirical MGFs.

426 *Encroachment re-surveys*

427 Finally, we used re-survey data from permanent transects to assess the predictions of
428 the SIPM with respect to independent empirical observations. In summer 2001, shrub
429 percent cover was recorded along two permanent 1000-m transects that spanned the
430 shrub-grass ecotone (these were different transects than those described above for shrub
431 demography). Surveys were conducted again in summer 2013 to document change in cre-
432 osotebush abundance and spatial extent. At every 10 meters, shrub cover was recorded
433 in nine cover classes (<1%, 1–4%, 5–10%, 10–25%, 25–33%, 33–50%, 50–75%, 75–95%,
434 >95%). For visualization, we show midpoint values of these cover classes at each meter
435 location for both transects and years.

436 **Results**

437 *Size and density dependent demography*

438 Demographic data from naturally occurring and transplanted individuals revealed strong
439 size- and density-dependence in demographic vital rates. For most sizes and vital rates,
440 shrub density had negative demographic effects; there was no strong evidence for posi-
441 tive density dependence in any demographic process at any size. Statistical support for
442 size- and density-dependence is provided in Tables ??–??, which provide AIC rankings
443 for candidate models based on the complete data set.

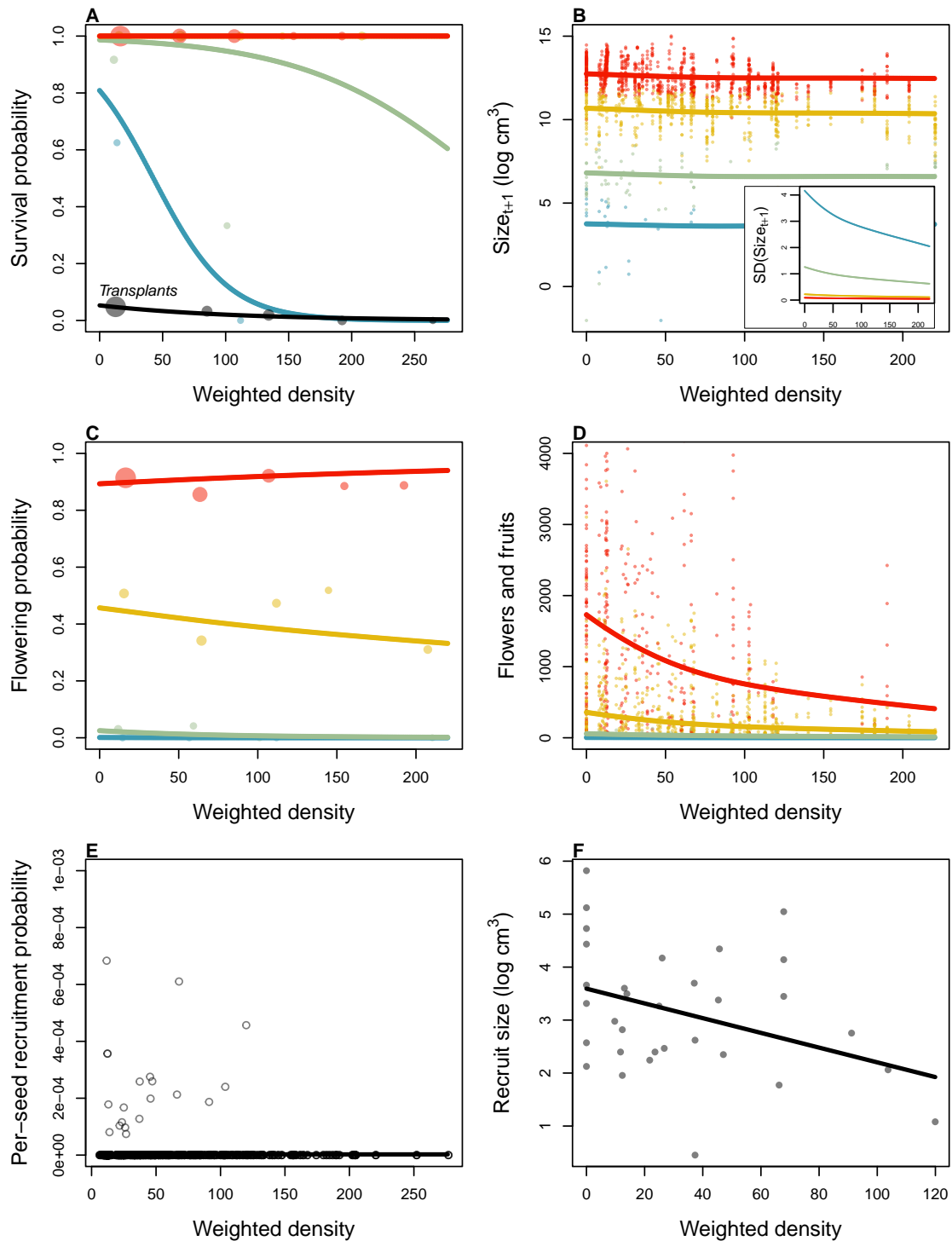


Figure 2: Size- and density-dependence in demographic vital rates. **A** Probability of survival from natural population census and transplant experiment (black line), **B** Mean and variance (inset) of size conditional on previous size, **C** Probability of flowering, **D** Flower and fruit production, **E** Probability of recruitment per seed, **F** Recruit size. In **A–E**, colored lines indicate four size groups (red is largest, blue is smallest), discretized for data visualization only. In all panels, weighted density is the sum of all plant sizes $\log(\text{cm}^3)$ within the same 5-m window as the census individual.

444 *Survival.* Among naturally occurring plants, survival of large, established individuals
445 was very high (Fig. 2A). We observed relatively few mortality events and nearly all of
446 these were among new recruits. The probability of survival at these small sizes declined
447 with increasing density. Survival of transplants was very low, lower even than survival
448 of similarly-sized, naturally occurring recruits (Fig. 2B). However, the transplant results
449 support the general pattern of negative density dependence in survival. Among the
450 20 survivors, 15 of them occurred in transect windows below the median of weighted
451 shrub density. In Appendix XX, we show that transplant mortality was dominated by
452 negative effects of shrub density at the 5-m window scale, even when effects of local grass
453 and shrub cover were included as alternative or additional statistical covariates, which
454 suggests that this is the appropriate spatial scale for modeling density dependence in
455 this system.

456 *Growth.* Current size was strongly predictive of future size, as expected, and there was
457 weak negative density dependence in mean future size conditioned on current size (Fig.
458 2C). However, there was a stronger signal of density dependence in the variance of fu-
459 ture size (Fig. 2C, inset). Plants at low density exhibited greater variance in growth
460 trajectories and this was especially true at the smallest sizes. Thus, large increases (and
461 decreases) in the size of new recruits were most likely to occur under low-density condi-
462 tions.

463 *Flowering and fruit production.* Flowering probability was strongly size-dependent and
464 and very weakly sensitive to local density (Fig. 2D). However, fertility of flowering plants
465 was strongly negative density dependent, with greatest flower and fruit production by
466 the largest plants at the lowest densities, and vice versa (Fig. 2E).

467 *Recruitment and recruit size.* We observed 32 natural recruitment events along our tran-
468 sects during the study years and our estimate recruitment rate, given total expected seed
469 production in each window preceding the recruitment year, was very low (2.47×10^{-6} ,
470 2E). While most recruitment events occurred at low density, this is also where most seed
471 production was concentrated (Fig. 2E) and low-density windows were over-represented
472 relative to high density. For these reasons we were more likely to observe recruitment
473 events at low density. Controlling for sampling effort and seed production, the sta-
474 tistical models indicated that our data were most consistent with a constant, density-
475 independent recruitment rate (Table XX). However, the mean size of new recruits de-
476 clined significantly with local density (Fig. 2F).

477 *Population growth rate.* As expected given the vital rate results, the asymptotic popula-
478 tion growth rate λ declined monotonically with density (Fig. 3). This was true across
479 nearly all bootstrap replicates, indicating high certainty that shrub fitness is maximized at
480 zero density and thus that the expansion wave is “pulled” (for this reason our wavespeed
481 results are based on the analytical approach described above). Mean growth rate at low
482 density was 3% per year, with bootstrap uncertainty spanning 1–6%. At high density in
483 the core of the expansion wave, population growth rates approached $\lambda = 1$, indicating
484 population stasis driven by near-perfect survival and extremely rare recruitment.

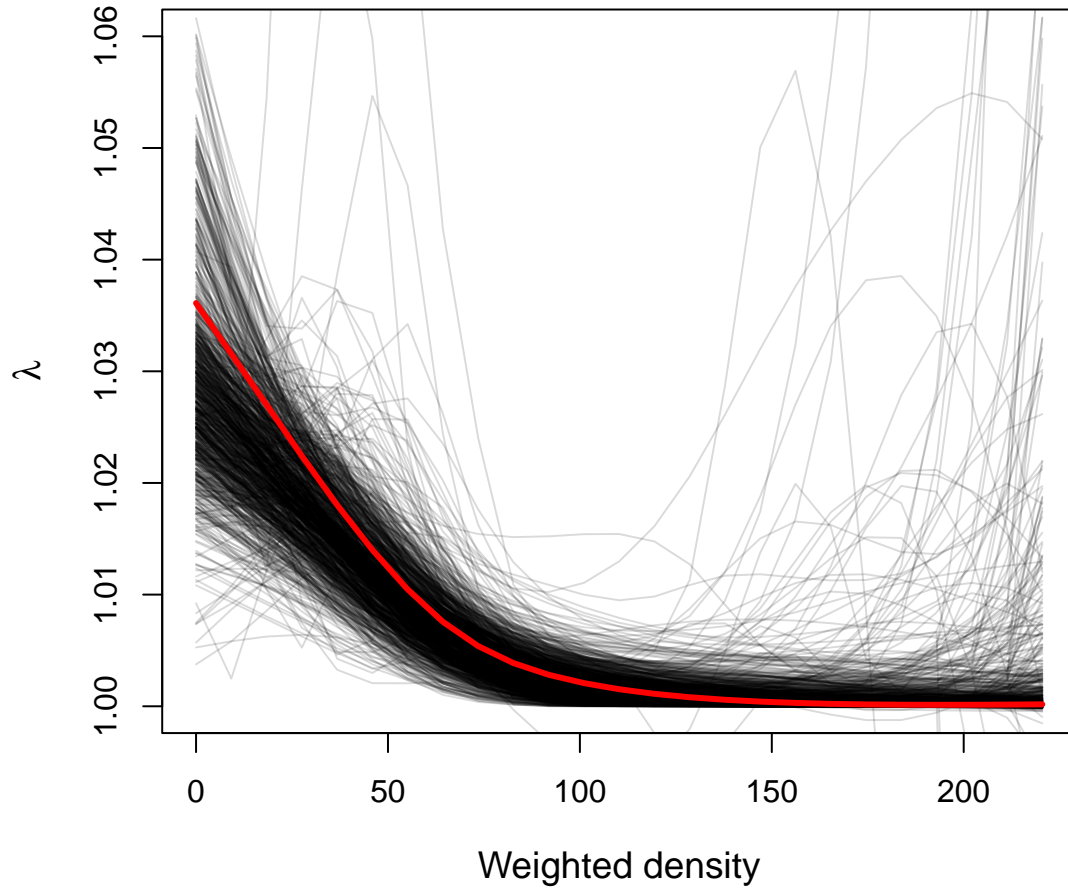


Figure 3: Density dependence in the asymptotic population growth rate (λ). Lines show bootstrap replicates sub-sampled from the full demographic data set. Weighted deighted density is the sum of all plant sizes $\log(\text{cm}^3)$ within 5-m windows.

Seed dispersal

485

486 WALD dispersal kernels, inferred from the properties of seeds and wind and account-
 487 ing for observed variation in wind speeds and within-plant seed release height, were
 488 predicted to be strongly size dependent, with taller plants having a greater probability

489 of dispersing seeds longer distances (Fig. 4). However, predicted seed dispersal was
490 highly local, with most seeds expected to fall within one meter of parent plants for most
491 sizes. Even for the very tallest shrub we observed (1.96 m), only 6.2% of its seeds were
492 predicted to fall more than 3 m away and less than 1% were predicted to fall more than
493 6 m away (Fig. 4). Taller shrubs also exhibited wider variance in their dispersal kernel
494 and this reflects their wider range of seed release heights.

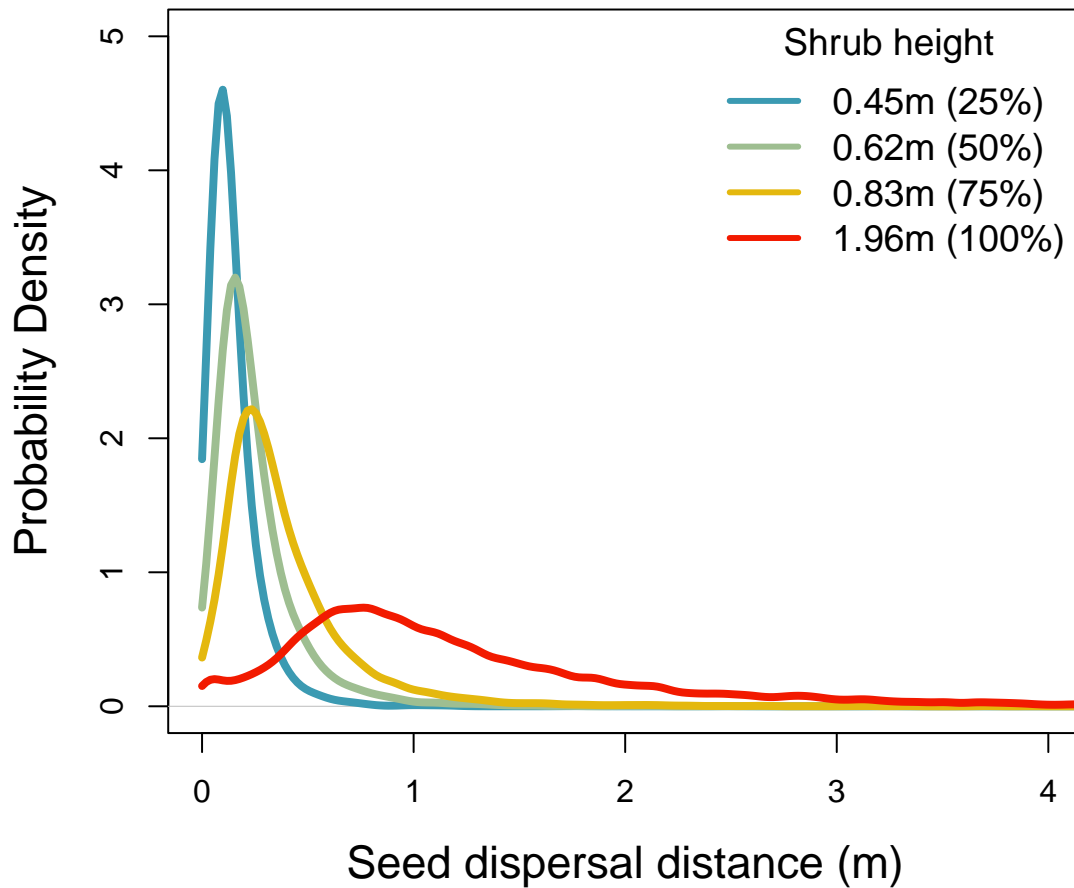


Figure 4: Predicted WALD dispersal kernels for four shrub heights corresponding to the 25th, 50th, 75th, and 100th (maximum) percentiles of the observed size distribution. We assume that heights below 15 cm have effectively no seed movement due to interference with the grass layer.

Expansion speed and sensitivities

495

496 The asymptotic speed of creosote encroachment, given the above demography and dis-
 497 persal patterns, was very slow. The mean asymptotic speed was VALUE m/year and
 498 the 5–95 percentiles of the uncertainty distribution was VALUE m/year (Fig. 6A). Ex-

499 pansion speed was by far the most sensitive to the probability of seedling recruitment
500 (Fig. 6B), indicating that this life cycle transition is imposes the strongest constraint on
501 encroachment. Sensitivity to survival ranked second, and since nearly all mortality oc-
502 curred at the smallest sizes this too can be interpreted as an early life cycle constraint on
503 expansion.

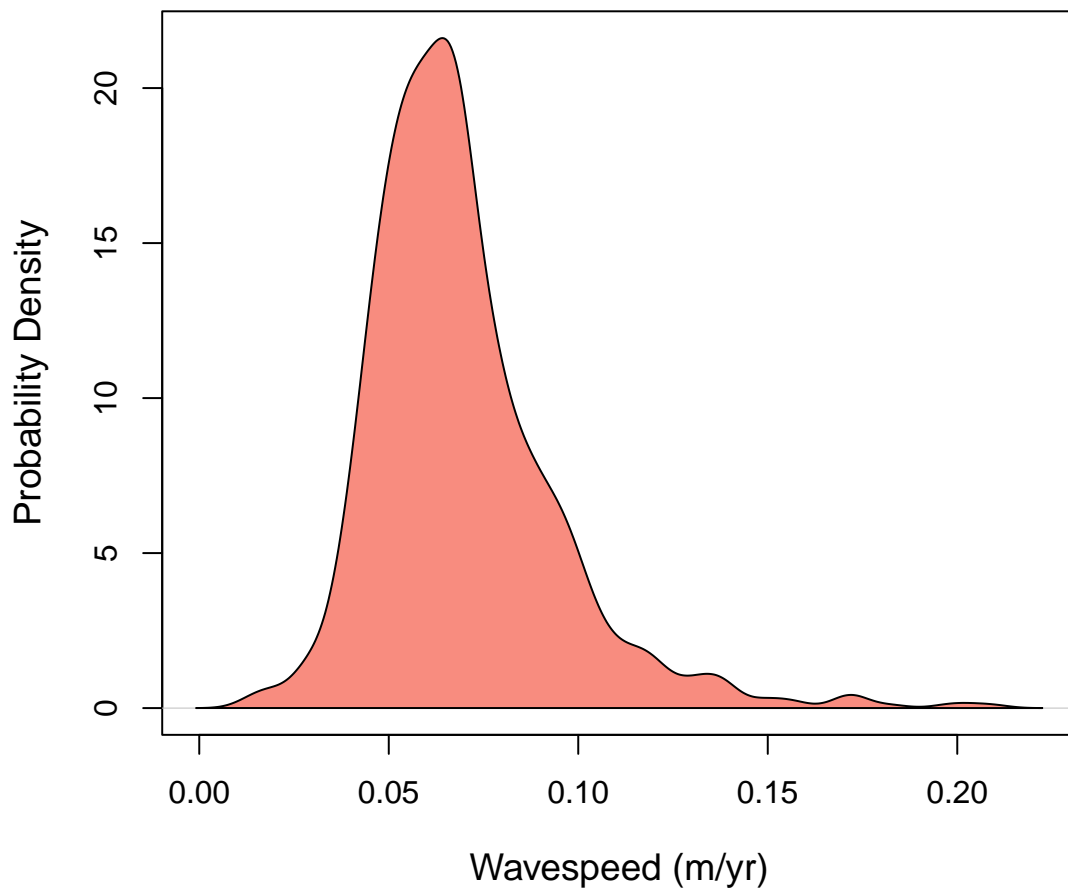


Figure 5: Estimated encroachment wave speeds (left) and geometric rates of population growth (right) for higher post-rainfall seedling survival and normal conditions.

504

Transect re-surveys

505 Re-surveys along two permanent transects revealed virtually no change the in the cre-
 506 osote expansion wave over the 12 years that preceded our study. There were local
 507 changes in percent cover: on average cover increased by XX% between surveys. How-
 508 ever, there was no clear indication that the leading edge of the creosote shrubland has
 509 advanced (the modest right-ward shift on both transects is within the range of measure-
 510 ment error).

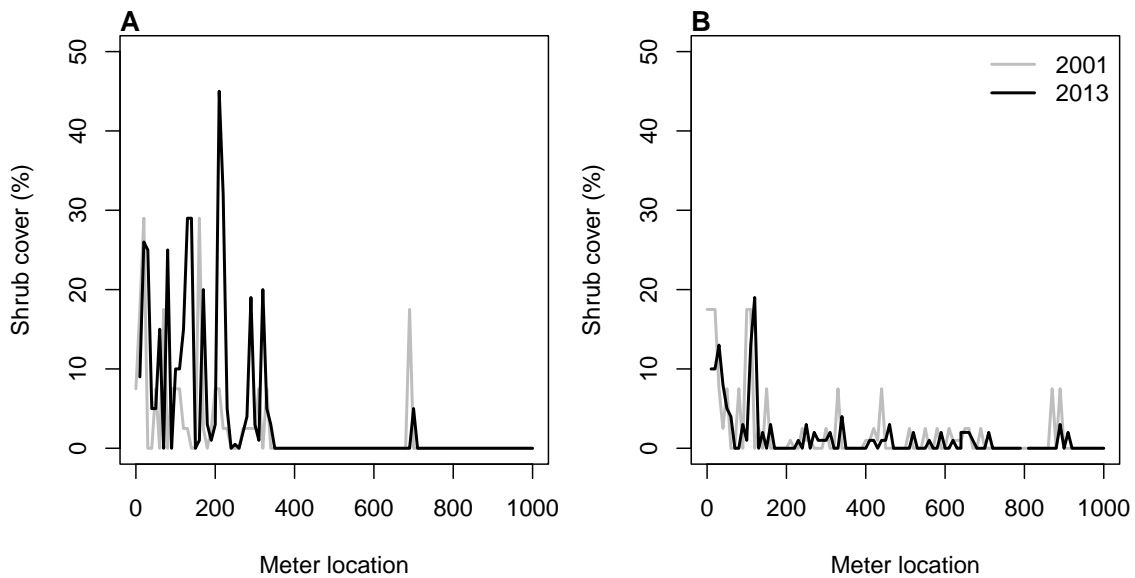


Figure 6: Surveys of creosotebush percent cover along two permanent transects (A,B) in 2001 and 2013.

511

Discussion

512 The encroachment of grasslands by woody plants is a worldwide phenomenon with
 513 broad implications for biodiversity and ecosystem function. To our knowledge, ours is

514 the first study to apply spatial population biology theory to woody plant encroachment.
515 This lens on the problem brings attention to the combined influence of dispersal and
516 density-dependent demography as critical controls on the occurrence and pace of en-
517 croachment. Through this lens, we asked whether the encroachment process is pushed
518 or pulled, hypothesizing that positive feedbacks, well documented in this and other
519 woody encroachment systems, would cause declines in fitness at the low-density front
520 and generate pushed-wave dynamics. Instead, observational and experimental evidence
521 unambiguously indicate that fitness was maximized in low-density plant neighborhoods.
522 The creosote encroachment wave is therefore predicted to be pulled by maximum de-
523 mographic performance at the leading edge. However, our field-parameterized spatial
524 integral projection model revealed that this wave is pulled at the very slow rate of 5–
525 10 centimeters per year – so slow that, under the observed conditions, this grass-shrub
526 ecotone is effectively stationary. Re-surveys of permanent transects independently sup-
527 ported this prediction, showing virtually no change in the position of the shrub boundary
528 in over a decade. Below, we discuss and interpret these key findings in greater detail.

529 Strong observational and experimental evidence for strictly negative density depen-
530 dence, in all vital rates and at all sizes, was surprising given widespread evidence for
531 positive feedbacks during woody plant encroachment generally (D’odorico et al., 2013)
532 and specifically in this system (D’Odorico et al., 2010). How can we square these appar-
533 ently conflicting results? First, it may be important to consider the distinction between
534 “demographic” and “component” Allee effects (Stephens et al., 1999), which refer to
535 effects that manifest in total fitness and components of fitness, respectively. That is,
536 positive effects of conspecific density may occur but in our measures of demographic
537 performance these are swamped by counter-acting negative effects. It is worth noting
538 that our demographic measurements are relatively coarse, reflecting aggregate perfor-

539 mance over a full transition year. More mechanistic studies on finer time scales might
540 reveal component Allee effects that are masked by strong net-negative density depen-
541 dence. Second, many of the possible mechanisms for positive feedbacks at shrub-grass
542 ecotones would manifest infrequently under extreme conditions. For example,

543 **Acknowledgements**

544 **Author contributions**

545 **Data accessibility**

546 **Literature Cited**

547 Bowers, J. E., R. M. Turner, and T. L. Burgess. 2004. Temporal and spatial patterns in
548 emergence and early survival of perennial plants in the Sonoran Desert. *Plant Ecology*
549 **172**:107–119.

550 Boyd, R. S., and G. D. Brum. 1983. Postdispersal reproductive biology of a Mojave Desert
551 population of *Larrea tridentata* (Zygophyllaceae). *American Midland Naturalist* pages
552 25–36.

553 Brandt, J. S., M. A. Haynes, T. Kuemmerle, D. M. Waller, and V. C. Radeloff. 2013.
554 Regime shift on the roof of the world: Alpine meadows converting to shrublands in
555 the southern Himalayas. *Biological Conservation* **158**:116–127.

556 Buffington, L. C., and C. H. Herbel. 1965. Vegetational changes on a semidesert grassland
557 range from 1858 to 1963. *Ecological monographs* **35**:139–164.

558 Bullock, J. M., S. M. White, C. Prudhomme, C. Tansey, R. Perea, and D. A. Hooftman.

2012. Modelling spread of British wind-dispersed plants under future wind speeds in
a changing climate. *Journal of Ecology* **100**:104–115.

Cabral, A., J. De Miguel, A. Rescia, M. Schmitz, and F. Pineda. 2003. Shrub encroachment
in Argentinean savannas. *Journal of Vegetation Science* **14**:145–152.

D’Odorico, P., J. D. Fuentes, W. T. Pockman, S. L. Collins, Y. He, J. S. Medeiros,
S. DeWekker, and M. E. Litvak. 2010. Positive feedback between microclimate and
shrub encroachment in the northern Chihuahuan desert. *Ecosphere* **1**:1–11.

D’Odorico, P., Y. He, S. Collins, S. F. De Wekker, V. Engel, and J. D. Fuentes. 2013.
Vegetation–microclimate feedbacks in woodland–grassland ecotones. *Global Ecology
and Biogeography* **22**:364–379.

D’Odorico, P., G. S. Okin, and B. T. Bestelmeyer. 2012. A synthetic review of feedbacks
and drivers of shrub encroachment in arid grasslands. *Ecohydrology* **5**:520–530.

Ellner, S. P., D. Z. Childs, M. Rees, et al. 2016. Data-driven modelling of structured
populations. *A practical guide to the Integral Projection Model*. Cham: Springer .

Gandhi, S. R., E. A. Yurtsev, K. S. Korolev, and J. Gore. 2016. Range expansions transition
from pulled to pushed waves as growth becomes more cooperative in an experimental
microbial population. *Proceedings of the National Academy of Sciences* **113**:6922–6927.

Gardner, J. L. 1951. Vegetation of the creosotebush area of the Rio Grande Valley in New
Mexico. *Ecological Monographs* **21**:379–403.

Gibbens, R., R. McNeely, K. Havstad, R. Beck, and B. Nolen. 2005. Vegetation changes in
the Jornada Basin from 1858 to 1998. *Journal of Arid Environments* **61**:651–668.

- Goslee, S., K. Havstad, D. Peters, A. Rango, and W. Schlesinger. 2003. High-resolution images reveal rate and pattern of shrub encroachment over six decades in New Mexico, USA. *Journal of Arid Environments* **54**:755–767.
- Grover, H. D., and H. B. Musick. 1990. Shrubland encroachment in southern New Mexico, USA: an analysis of desertification processes in the American Southwest. *Climatic change* **17**:305–330.
- Hsieh, C.-I., and G. G. Katul. 1997. Dissipation methods, Taylor’s hypothesis, and stability correction functions in the atmospheric surface layer. *Journal of Geophysical Research: Atmospheres* **102**:16391–16405.
- Huang, H., L. D. Anderegg, T. E. Dawson, S. Mote, and P. D’Odorico. 2020. Critical transition to woody plant dominance through microclimate feedbacks in North American coastal ecosystems. *Ecology* **101**:e03107.
- Jongejans, E., K. Shea, O. Skarpaas, D. Kelly, and S. P. Ellner. 2011. Importance of individual and environmental variation for invasive species spread: a spatial integral projection model. *Ecology* **92**:86–97.
- Katul, G., A. Porporato, R. Nathan, M. Siqueira, M. Soons, D. Poggi, H. Horn, and S. A. Levin. 2005. Mechanistic analytical models for long-distance seed dispersal by wind. *The American Naturalist* **166**:368–381.
- Keitt, T. H., M. A. Lewis, and R. D. Holt. 2001. Allee effects, invasion pinning, and species’ borders. *The American Naturalist* **157**:203–216.
- Kelleway, J. J., K. Cavanaugh, K. Rogers, I. C. Feller, E. Ens, C. Doughty, and N. Saintilan. 2017. Review of the ecosystem service implications of mangrove encroachment into salt marshes. *Global Change Biology* **23**:3967–3983.

603 Knapp, A. K., J. M. Briggs, S. L. Collins, S. R. Archer, M. S. BRET-HARTE, B. E. Ewers,
604 D. P. Peters, D. R. Young, G. R. Shaver, E. Pendall, et al. 2008. Shrub encroachment in
605 North American grasslands: shifts in growth form dominance rapidly alters control of
606 ecosystem carbon inputs. *Global Change Biology* **14**:615–623.

607 Kot, M., M. A. Lewis, and P. van den Driessche. 1996. Dispersal data and the spread of
608 invading organisms. *Ecology* **77**:2027–2042.

609 Lewis, M., and P. Kareiva. 1993. Allee dynamics and the spread of invading organisms.
610 *Theoretical Population Biology* **43**:141–158.

611 Lewis, M. A., M. G. Neubert, H. Caswell, J. S. Clark, and K. Shea, 2006. A guide to cal-
612 culating discrete-time invasion rates from data. Pages 169–192 *in* *Conceptual ecology*
613 *and invasion biology: reciprocal approaches to nature*. Springer.

614 Mabry, T. J., J. H. Hunziker, D. Difeo Jr, et al. 1978. Creosote bush: biology and chemistry
615 of *Larrea* in New World deserts. Dowden, Hutchinson & Ross, Inc.

616 Maddox, J. C., and S. Carlquist. 1985. Wind dispersal in Californian desert plants:
617 experimental studies and conceptual considerations. *Aliso: A Journal of Systematic*
618 *and Evolutionary Botany* **11**:77–96.

619 Moore, D., and K. Hall, 2022. Meteorology Data from the Sevilleta Na-
620 tional Wildlife Refuge, New Mexico. Environmental Data Initiative.
621 <https://doi.org/10.6073/pasta/d56307b398e28137dabaa6994f0f5f92>.

622 Moreno-de las Heras, M., L. Turnbull, and J. Wainwright. 2016. Seed-bank structure
623 and plant-recruitment conditions regulate the dynamics of a grassland-shrubland Chi-
624 huahuan ecotone. *Ecology* **97**:2303–2318.

- 625 Mugasi, S., E. Sabiiti, and B. Tayebwa. 2000. The economic implications of bush en-
626 croachment on livestock farming in rangelands of Uganda. *African Journal of Range*
627 *and Forage Science* **17**:64–69.
- 628 Nathan, R., G. G. Katul, G. Bohrer, A. Kupařinen, M. B. Soons, S. E. Thompson, A. Trakht-
629 enbrot, and H. S. Horn. 2011. Mechanistic models of seed dispersal by wind. *Theoret-*
630 *ical Ecology* **4**:113–132.
- 631 Neubert, M. G., and H. Caswell. 2000. Demography and dispersal: calculation and
632 sensitivity analysis of invasion speed for structured populations. *Ecology* **81**:1613–
633 1628.
- 634 Oba, G., E. Post, P. Syvertsen, and N. Stenseth. 2000. Bush cover and range condition
635 assessments in relation to landscape and grazing in southern Ethiopia. *Landscape*
636 *ecology* **15**:535–546.
- 637 Pan, S., and G. Lin. 2012. Invasion traveling wave solutions of a competitive system with
638 dispersal. *Boundary Value Problems* **2012**:120.
- 639 Parizek, B., C. M. Rostagno, and R. Sottini. 2002. Soil erosion as affected by shrub
640 encroachment in northeastern Patagonia. *Rangeland Ecology & Management/Journal*
641 *of Range Management Archives* **55**:43–48.
- 642 Peters, D. P., and J. Yao. 2012. Long-term experimental loss of foundation species:
643 consequences for dynamics at ecotones across heterogeneous landscapes. *Ecosphere*
644 **3**:1–23.
- 645 Ratajczak, Z., J. B. Nippert, and S. L. Collins. 2012. Woody encroachment decreases
646 diversity across North American grasslands and savannas. *Ecology* **93**:697–703.

- 647 Raupach, M. 1994. Simplified expressions for vegetation roughness length and zero-
648 plane displacement as functions of canopy height and area index. *Boundary-Layer*
649 *Meteorology* **71**:211–216.
- 650 Ravi, S., P. D’Odorico, S. L. Collins, and T. E. Huxman. 2009. Can biological invasions
651 induce desertification? *The New Phytologist* **181**:512–515.
- 652 Reed, M., L. Stringer, A. Dougill, J. Perkins, J. Atlhopheng, K. Mulale, and N. Favretto.
653 2015. Reorienting land degradation towards sustainable land management: Linking
654 sustainable livelihoods with ecosystem services in rangeland systems. *Journal of envi-*
655 *ronmental management* **151**:472–485.
- 656 Reynolds, J. F., R. A. Virginia, P. R. Kemp, A. G. De Soyza, and D. C. Tremmel. 1999.
657 Impact of drought on desert shrubs: effects of seasonality and degree of resource
658 island development. *Ecological Monographs* **69**:69–106.
- 659 Roques, K., T. O’connor, and A. R. Watkinson. 2001. Dynamics of shrub encroachment in
660 an African savanna: relative influences of fire, herbivory, rainfall and density depen-
661 dence. *Journal of Applied Ecology* **38**:268–280.
- 662 Schlesinger, W. H., and A. M. Pilmanis. 1998. Plant-soil interactions in deserts. *Biogeo-*
663 *chemistry* **42**:169–187.
- 664 Schlesinger, W. H., J. A. Raikes, A. E. Hartley, and A. F. Cross. 1996. On the spatial
665 pattern of soil nutrients in desert ecosystems: ecological archives E077-002. *Ecology*
666 **77**:364–374.
- 667 Schlesinger, W. H., J. F. Reynolds, G. L. Cunningham, L. F. Huenneke, W. M. Jarrell, R. A.
668 Virginia, and W. G. Whitford. 1990. Biological feedbacks in global desertification.
669 *Science* **247**:1043–1048.

- 670 Sirami, C., and A. Monadjem. 2012. Changes in bird communities in Swaziland savannas
671 between 1998 and 2008 owing to shrub encroachment. *Diversity and Distributions*
672 **18**:390–400.
- 673 Skarpaas, O., and K. Shea. 2007. Dispersal patterns, dispersal mechanisms, and invasion
674 wave speeds for invasive thistles. *The American Naturalist* **170**:421–430.
- 675 Stephens, P. A., W. J. Sutherland, and R. P. Freckleton. 1999. What is the Allee effect?
676 *Oikos* pages 185–190.
- 677 Sullivan, L. L., B. Li, T. E. Miller, M. G. Neubert, and A. K. Shaw. 2017. Density depen-
678 dence in demography and dispersal generates fluctuating invasion speeds. *Proceed-*
679 *ings of the National Academy of Sciences* **114**:5053–5058.
- 680 Taylor, C. M., and A. Hastings. 2005. Allee effects in biological invasions. *Ecology Letters*
681 **8**:895–908.
- 682 Trollope, W., F. Hobson, J. Danckwerts, and J. Van Niekerk. 1989. Encroachment and
683 control of undesirable plants. *Veld management in the Eastern Cape* pages 73–89.
- 684 Turnbull, L., J. Wainwright, and R. E. Brazier. 2010. Changes in hydrology and erosion
685 over a transition from grassland to shrubland. *Hydrological Processes: An Interna-*
686 *tional Journal* **24**:393–414.
- 687 Van Auken, O. 2009. Causes and consequences of woody plant encroachment into
688 western North American grasslands. *Journal of environmental management* **90**:2931–
689 2942.
- 690 Van Auken, O. W. 2000. Shrub invasions of North American semiarid grasslands. *Annual*
691 *review of ecology and systematics* **31**:197–215.

- 692 Vasek, F. C. 1980. Creosote bush: Long-lived clones in the Mojave Desert. *American*
693 *Journal of Botany* **67**:246–255.
- 694 Veit, R. R., and M. A. Lewis. 1996. Dispersal, population growth, and the Allee effect: dy-
695 namics of the house finch invasion of eastern North America. *The American Naturalist*
696 **148**:255–274.
- 697 Wang, M.-H., M. Kot, and M. G. Neubert. 2002. Integrodifference equations, Allee effects,
698 and invasions. *Journal of mathematical biology* **44**:150–168.
- 699 Wiernga, J. 1993. Representative roughness parameters for homogeneous terrain.
700 *Boundary-Layer Meteorology* **63**:323–363.
- 701 Williams, J. L., T. E. Miller, and S. P. Ellner. 2012. Avoiding unintentional eviction from
702 integral projection models. *Ecology* **93**:2008–2014.
- 703 Wood, S. 2017. *Generalized Additive Models: An Introduction with R*. 2 edition. Chap-
704 man and Hall/CRC.

Appendix A: Dispersal kernel modeling

WALD dispersal kernel. In order to create the dispersal kernel, we first take the wind speeds at measurement height z_m and correct them to find wind speed U for any height H by using the logarithmic wind profile ⁵

$$U = \frac{1}{H} \int_{d+z_0}^H \frac{u^*}{K} \log \left(\frac{z-d}{z_0} \right) dz \quad (\text{A1})$$

given in Bullock et al. (2012) equation 6, with the notation slightly modified. Here, z is the height above the ground, K is the von Karman constant, and u^* is the friction velocity. The zero-plane displacement d and roughness length z_0 are surface roughness parameters that, for a grass canopy height h above the ground, are approximated by $d \approx 0.7h$ and $z_0 \approx 0.1h$. These estimates are from Raupach (1994) for a canopy area index $\Lambda = 1$ in which the sum of grass canopy elements is equal to the unit area being measured. A 0.15 m grass height at our study site gives $d = 0.105$ and z_0 , which are suitable approximations for grassland (Wiernga, 1993). Calculations of u^* were done using equation A2 from Skarpaas and Shea (2007), in which

$$u^* = KU_m \left[\log \left(\frac{z_m - d}{z_0} \right) \right]^{-1} \quad (\text{A2})$$

and U_m is the mean wind velocity at the measurement height z_m . Values for the turbulent flow parameter σ were then calculated using the estimate made by Skarpaas and Shea (2007) in their equation A4, where

$$\sigma = 2A_w^2 \sqrt{\frac{K(z-d)u^*}{C_0 U}} \quad (\text{A3})$$

⁵We need to describe and cite the wind data used here.

724 and C_0 is the Kolmogorov constant. A_w is a constant that relates vertical turbulence
725 to friction velocity and is approximately equal to 1.3 under the assumptions of above-
726 canopy flow made by Skarpaas and Shea (2007), based off calculations from Hsieh and
727 Katul (1997). In addition, the assumption that $z = H$ was made in order to make the
728 calculation of σ more feasible.⁶

729 The values from the previous three equations give us the necessary information to
730 calculate μ' and λ' , thus allowing us to create the WALD distribution $p(r)$. However, the
731 base WALD model does not take into account variation in wind speeds or seed terminal
732 velocities, which limits its applicability in systems where such variation is present. In
733 order to account for this variation, we integrate the WALD model over distributions of
734 these two variables using the same method as Skarpaas and Shea (2007). Additionally,
735 the WALD model assumes seed release from a single point source, which is not realistic
736 for creosote bush; because seeds are released across the entire height of the shrub rather
737 than from a point source, we integrated $p(r)$ across the uniform distribution from the
738 grass canopy height to the shrub height. Thus, under the assumptions that the height at
739 which a seed is located does not affect its probability of being released and that seeds
740 are evenly distributed throughout the shrub, this gives the dispersal kernel $K(r)$, where

$$741 \quad K(r) = \iiint p(F)p(U)p(z)p(r) dF dU dz \quad (A4)$$

742 and $p(F)$ and $p(U)$ are the PDFs of the terminal velocity F and wind speed U , re-
743 spectively, and $p(z)$ is the uniform distribution from h to H .

744 *Dispersal data collection.* The distribution $p(F)$ in the integral above was constructed
745 using experimentally determined seed terminal velocities. This was done by using

⁶Can you describe this assumption in biological terms?

laboratory-based seed release experiments with a high-speed camera and motion tracking software to determine position as a function of time. We then used the Levenberg-Marquardt algorithm to solve a quadratic-drag equation of motion for F . Before seeds were released, they were dried, dyed with yellow fluorescent powder, and then put against a black background to improve visibility and make tracking easier. While the powder added mass to the seeds, this added mass only yielded an approximately 2.5% increase, likely having little effect on terminal velocities. Measurements were conducted for 48 seeds that were randomly chosen from a seed pool derived from different plants, and then an empirical PDF of terminal velocities was constructed using the data. Constructing $p(U)$ involved creating an empirical PDF of hourly wind speeds using data from Sevilleta LTER meteorological station 49, the station closest to our transects. We used wind speed data collected hourly from 2015 to 2019 (Moore and Hall, 2022).

Appendix B: Additional results

```
## Error in xtable(aic_tables$surv_aic_out[, c("surv", "df", "dAIC")], caption
= "AIC model selection for survival probability.", : object 'aic_tables' not
found
```

```
## Error in align(surv_aic) <- "c|p{12cm}|c|c|": object 'surv_aic' not found
```

```
## Error in print(surv_aic, include.rownames = F, include.colnames = T, floating
= TRUE, : object 'surv_aic' not found
```

```
## Error in xtable(aic_tables$grow_aic_out[, c("mean(size)", "sd(size)", : object
'aic_tables' not found
```

```
## Error in align(grow_aic) <- "c|p{8cm}|p{4cm}|c|c|": object 'grow_aic' not
found
```

```
## Error in print(grow_aic, include.rownames = F, include.colnames = T, floating
= TRUE, : object 'grow_aic' not found
```

```
## Error in xtable(aic_tables$flower_aic_out[, c("Pr(Flowering)", "df", "dAIC")],
: object 'aic_tables' not found
```

```
## Error in align(flower_aic) <- "c|p{8cm}|c|c|": object 'flower_aic' not found
```

```
## Error in print(flower_aic, include.rownames = F, include.colnames = T, : object
'flower_aic' not found
```

```
## Error in xtable(aic_tables$fruits_aic_out[, c("No. fruits", "df", "dAIC")],
```

```

: object 'aic_tables' not found

## Error in align(fruits_aic) <- "c|p{8cm}|c|c|": object 'fruits_aic' not found
## Error in print(fruits_aic, include.rownames = F, include.colnames = T, : object
'fruits_aic' not found

## Error in xtable(aic_tables$recruit_aic_out[, c("Pr(Recruitment)", "df", :
object 'aic_tables' not found
## Error in align(recruit_aic) <- "c|p{8cm}|c|c|": object 'recruit_aic' not
found
## Error in print(recruit_aic, include.rownames = F, include.colnames = T, :
object 'recruit_aic' not found

## Error in xtable(aic_tables$recruitsize_aic_out[, c("mean(size)", "sd(size)",
: object 'aic_tables' not found
## Error in align(recruitsize_aic) <- "c|p{8cm}|p{4cm}|c|c|": object 'recruitsize_aic'
not found
## Error in print(recruitsize_aic, include.rownames = F, include.colnames = T,
: object 'recruitsize_aic' not found

```

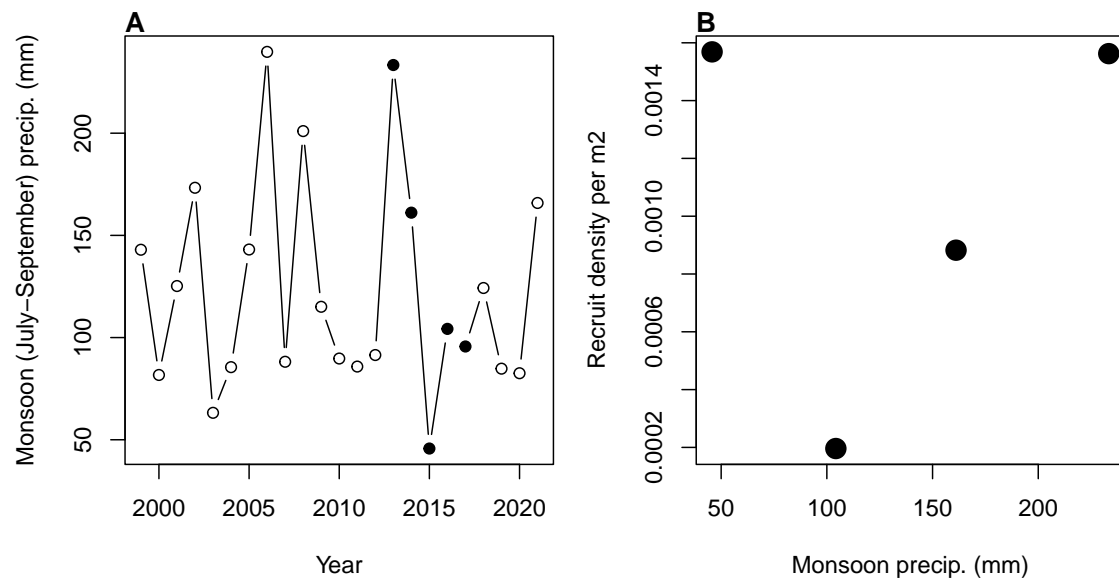


Figure B1: .